Polymer Chemistry

PAPER

View Article Online
View Journal | View Issue

Cite this: *Polym. Chem.*, 2017, **8**, 2235

Free-standing thermo-responsive nanoporous membranes from high molecular weight PS-PNIPAM block copolymers synthesized *via* RAFT polymerization†

Merve Cetintas,[a] Joris de Grooth,[b] Anton H. Hofman,[c] Hanne M. van der Kooij,[a] Katja Loos,[c] Wiebe M. de Vos[b] and Marleen Kamperman *[a]

The incorporation of stimuli-responsive pores in nanoporous membranes is a promising approach to facilitate the cleaning process of the membranes. Here we present fully reversible thermo-responsive nanoporous membranes fabricated by self-assembly and non-solvent induced phase separation (SNIPS) of polystyrene-poly(*N*-isopropylacrylamide) (PS-PNIPAM) block copolymers. A variety of PS-PNIPAM block copolymers were synthesized by reversible addition–fragmentation chain transfer (RAFT) polymerization and the reaction conditions were optimized. The target copolymers featured: (1) a thermo-responsive PNIPAM block, (2) a majority PS fraction, and (3) a well-defined high molecular weight, which are requirements for successful fabrication of free-standing responsive membranes using SNIPS. The resulting membranes exhibited a worm-like cylindrical morphology with interconnected nanopores. The thermo-responsive character of the membranes was studied by measuring the permeability of the membranes as a function of temperature. The permeability was found to increase by almost 400% upon going from room temperature to 50 °C and this thermo-responsive character was fully reversible.

Received 5th January 2017,
Accepted 16th March 2017

DOI: 10.1039/c7py00023e

rsc.li/polymers

Introduction

Fouling, both biological and colloidal in nature, can be considered as one of the biggest challenges in membrane technology. It is the process where biomolecules, cells or suspended particles deposit reversibly or irreversibly on the membrane surface leading to reductions in flux and/or in the separation quality, and consequently in reduced production capacity and increased operation costs. Fouling can especially be a problem for membranes with small pore sizes (below 20 nm), because cleaning (using *e.g.* back flushing) is more challenging due to low shear forces that can be achieved in such small pores. To reduce this problem, by facilitating the cleaning process of the membranes, several methods have been developed.[1] A promising approach is the incorporation of stimuli-responsive pores into the membrane, which can be achieved by using polymers having a stimuli-responsive character.[2–19] Upon the application of an external stimulus, *e.g.* thermal, pH, light, magnetic or electrical, the size of the pores increases. This in turn allows for higher back flush speeds and thus for higher shear forces that leads to much more efficient physical cleaning.[2,9,10,15,20,21]

Block copolymers (BCPs) are an interesting class of materials for nanoporous membrane applications, as block copolymer self-assembly can lead to the formation of monodisperse nanopores.[22–31] Common methods for the fabrication of block copolymer membranes include spin-coating and a method called self-assembly and non-solvent induced phase separation (SNIPS). Spin-coating of a thin block copolymer layer on a porous support, or transferring the thin film to a porous support, is followed by annealing (and possible etching of one of the blocks) results in permeable films suitable for membrane applications.[32,33] Nykänen *et al.* reported that membranes prepared from a spin-coated polystyrene-*b*-poly(*N*-isopropylacrylamide)-*b*-polystyrene triblock copolymer showed thermo-responsive properties due to the poly(*N*-isopropylacrylamide) (PNIPAM) block exhibiting a lower critical solution temperature (LCST) of 32 °C.[34] Recently, another thermo-responsive membrane was obtained by spin-coating of poly (ethylene glycol methyl ether methacrylate)-*b*-polystyrene-*b*-poly(ethylene glycol methyl ether methacrylate) BCPs.[35]

[a]*Physical Chemistry and Soft Matter, Wageningen University & Research, Stippeneng 4, 6708 WE Wageningen, The Netherlands. E-mail: marleen.kamperman@wur.nl*
[b]*Membrane Science and Technology, MESA+ Institute for Nanotechnology, University of Twente, 7500 AE Enschede, The Netherlands*
[c]*Macromolecular Chemistry & New Polymeric Materials, Zernike Institute for Advanced Materials, University of Groningen, Nijenborgh 4, 9747 AG Groningen, The Netherlands*

†Electronic supplementary information (ESI) available. See DOI: 10.1039/c7py00023e

In SNIPS, a viscous polymer solution is cast on a substrate with a known wet thickness, followed by solvent evaporation to densify the membrane top layer and finally the polymer film is transferred into a non-solvent bath to form the desired porous structure.[36] The major advantage compared to spin-coating is that since the films are free-standing, a transfer of the membrane to a porous support step is not necessary for SNIPS membranes. Moreover, pores can be produced directly, without the need of additional steps such as etching of one of the blocks.

Polystyrene-*b*-poly(4-vinylpyridine) (PS-*b*-P4VP) block copolymer membranes produced by the SNIPS process were studied in detail due to the polymer's ability to self-assemble into isoporous structures and its pH-responsive behavior.[6,7,16,19,20,37,38] Despite the excellent results obtained for PS-*b*-P4VP copolymers, SNIPS is not limited to this copolymer and was extended to other responsive BCPs, including poly(isoprene-*b*-styrene-*b*-4-vinylpyridine)[17,18] polystyrene-*b*-poly(2-(dimethylamino)ethyl methacrylate)[5,11] and poly(styrene-*co*-isoprene)-*b*-poly(*N*,*N*-dimethylaminoethyl methacrylate).[8] The poly(*N*,*N*-dimethylaminoethyl methacrylate) containing membranes showed both pH- and thermo-responsive behavior. This dual responsive behavior was also obtained by Clodt *et al.* by coating a PNIPAM layer onto a pH-responsive PS-*b*-P4VP membrane.[3]

SNIPS of isoporous membranes is based on the formation of perpendicularly oriented cylinders after a short solvent evaporation step (<1 min) that results in isoporous surfaces after subsequent transfer into the non-solvent bath.[19,22,39] A worm-like cylindrical morphology with nanopores is an interesting alternative to the commonly employed isoporous morphology for nanoporous membranes, because it can be produced for a wide range of membrane casting parameter values.[38] In our study, we use BCPs containing polystyrene (PS) as the supporting block and thermo-responsive poly(*N*-isopropylacrylamide) (PNIPAM) to produce free-standing membranes by using SNIPS. Well-defined high molecular weight PS-PNIPAM BCPs were synthesized with a minority PNIPAM fraction using reversible addition–fragmentation chain transfer (RAFT) polymerization. RAFT polymerization was chosen since it yields well-defined polymer products using conventional free radical polymerization conditions.[40] RAFT is particularly attractive, because it was found to be one of the most suitable methods to produce NIPAM-containing polymers in a controlled fashion. For instance, atom transfer radical polymerization (ATRP) of acrylamides turned out to be challenging, since complexation of the copper catalyst to the amide group resulted in a higher concentration of active species, thus more termination and relatively high polydispersity index (PDI) values.[41] Anionic polymerization on the other hand is incompatible with acrylamides, and therefore makes it an unsuitable candidate for direct polymerization of unprotected NIPAM.[42] The synthesized PS-PNIPAM BCPs were used for the first time in a SNIPS process and free-standing membranes were successfully fabricated. The membranes exhibited a worm-like cylindrical morphology with nano-sized pores. By measuring the permeability values at different temperatures, it was shown that the membranes were thermo-responsive and that the thermo-responsive behavior was fully reversible.

Experimental

Materials

Styrene (Sigma-Aldrich, >99%) was vacuum distilled after stirring overnight over calcium hydride. *N*-Isopropylacrylamide (NIPAM) (Sigma-Aldrich, 97%) was purified by recrystallization from toluene. 2,2′-Azobis(2-methylpropionitrile) (AIBN) (Sigma-Aldrich, 98%) was recrystallized from methanol. Acetone, carbon disulphide (CS_2) (anhydrous, ≥99%), chloroform (anhydrous, ≥99%), 1,4-dioxane (anhydrous, 99.8%), NMR solvents (deuterated chloroform ($CDCl_3$) (99.96% D) and deuterated dimethyl sulphoxide-d_6 (DMSO-d_6) (99.96% D)) were purchased from Sigma-Aldrich and were used as received.

Synthesis procedures

Synthesis of *S*,*S*′-bis(α,α′-dimethyl-α″-acetic acid) trithiocarbonate (BDAT). A difunctional RAFT agent BDAT was synthesized using the method of Lai *et al.*[43] and characterized by ^{1}H and ^{13}C NMR. CS_2 (4.11 g), chloroform (16.12 g), acetone (7.85 g) and tetrabutylammonium bisulfate (0.36 g) were dissolved in mineral spirits (18 mL) in a jacketed reactor and cooled with tap water under N_2 atmosphere. After full dissolution, 50 wt% aqueous NaOH solution (30.24 g) was added dropwise over the course of 90 minutes to keep the temperature lower than 25 °C. After stirring overnight, water (135 mL) was added to dissolve the solid. To acidify the aqueous layer, concentrated HCl (18 mL) was added (*caution*: corrosive gas, mercaptan odor!). The reactor was purged with nitrogen for 30 min under continuous stirring. The solid was filtered and rinsed thoroughly with water. It was dried in a vacuum oven for two days at room temperature. The product was recrystallized from 60% acetone solution and dried in a vacuum oven for two days at room temperature giving yellow powder (1.2 g, 11%). Mp: 165 ± 3 °C (from 60% acetone, capillary method). ^{1}H NMR (400 MHz, DMSO-d_6): δ = 1.59 (12H, s, –CH_3), 12.91 (2H, s, –COOH). ^{13}C NMR (400 MHz, DMSO-d_6): δ = 25.76, 57.25, 176.26, 220.50.

Synthesis of PS macro-RAFT agents. Freshly distilled styrene, BDAT and AIBN were dissolved in 1,4-dioxane by stirring at room temperature. The solution was transferred to a Schlenk ampoule using syringes. After degassing by three successive freeze–pump–thaw cycles using a high vacuum Schlenk line, the solutions were heated to 70 °C by using a temperature controlled oil bath. The solution was allowed to polymerize for a certain amount of time. The reaction was stopped by cooling the ampoules in liquid nitrogen. The product was precipitated twice in cold methanol and dried in a vacuum oven at room temperature overnight to yield a white-yellowish powder (Table S1†). ^{1}H NMR (400 MHz, $CDCl_3$): δ = 6.2–7.1 (5H, m, Ph), 1.2–2.4 (3H, m, –CH–CH_2–) (Fig. S1†).

Synthesis of PS-*b*-PNIPAM-*b*-PS copolymers. The PS macro-RAFT agent, NIPAM and AIBN were dissolved in 1,4-dioxane. The solution was degassed by three successive freeze–pump–

Table 1 Synthesis conditions and characterization results of the obtained BCPs (synthesis conditions and characterization results of the macro-RAFT agents are given in Tables S1 and S2)

Copolymer	Reaction route in Scheme 1	Macro-RAFT	$\bar{M}_n$ macro-RAFT (kDa) (GPC)	$[M]_0$	$[M]_0/[\text{macro RAFT}]_0$	$[\text{Macro RAFT}]_0/[I]_0$	f_{PS} (wt%) (theory)	f_{PS} (wt%) (NMR)	$\bar{M}_n$ copolymer (kDa) (NMR)	PDI (GPC)	Yield (%)
CP-1	(1)	PS-1	57	0.68	750	5.8	39	45	127	1.40	30
CP-2	(1)	PS-1	57	0.68	35	5.8	95	89	64	1.83	13
CP-3	(1)	PS-8	110	0.32	204	3.5	90	69	159	1.40	1
CP-4	(1)	PS-9	92	0.28	177	3.5	90	100	—	—	—
CN-1	(2)	PN-1	41	4.35	1894	7.5	85	85	273	1.44	29
CN-2	(3)	PN-4	35	4.68	2656	10.0	85	87	269	1.36	18
CN-3	(3)	PN-5	25	4.35	1917	10.0	85	83	194	1.34	33
CN-4	(3)	PN-5	25	4.35	914	10.0	75	81	132	1.32	30

thaw cycles and heated in a temperature controlled oil bath to 70 °C for 18 h. Then the reaction was stopped by cooling the reaction mixture in liquid nitrogen. 1,4-Dioxane was removed with a rotary evaporator and dissolved in THF. The block copolymer was precipitated in diethyl ether and cold water, respectively. The precipitant obtained from diethyl ether precipitation was separated by centrifuging with Teflon centrifuge tubes and decantation. The product was separated from the homopolymer PNIPAM by centrifugation (45 min, 5000 rpm) three times. The purified copolymer was freeze-dried (Table 1). ^{1}H NMR (400 MHz, $CDCl_3$): δ = 6.2–7.1 (5H, m, Ph), 4.0 (1H, s, –NCH–), 0.8–2.5 (3H, m, –CH–CH_2– for PS and 9H, m, –CH_3, –CH–CH_2 for PNIPAM) (Fig. S2†).

Synthesis of PNIPAM macro-RAFT agents. Either a mono- or a difunctional RAFT agent were used for the synthesis of PNIPAM macro-RAFT agents, *i.e.* 2-(dodecylthiocarbonothioylthio)-2-methylpropionic acid (DTMA) and the previously synthesized *S*,*S*′-bis(α,α′-dimetyl-α″-aceticacid) trithiocarbonate (BDAT), respectively. AIBN, NIPAM and RAFT agent were dissolved in 1,4-dioxane. The solution was transferred to a Schlenk ampoule. After three freeze–pump–thaw cycles, the solution was heated to 70 °C for a certain time. The reaction was stopped by cooling the solution with liquid nitrogen. The solution was precipitated in diethyl ether and reprecipitated three times with cold ether after dissolution using a minimum amount of acetone. The product was dried overnight in a vacuum oven at room temperature (Table S2†). ^{1}H NMR (400 MHz, $CDCl_3$): δ = 4.0 (1H, s, –NCH–), 0.8–2.5 (9H, m, –CH_3, –CH–CH_2–), 5.8–7.5 (1H, br, –NH–) (Fig. S3†).

Synthesis of PNIPAM-*b*-PS-*b*-PNIPAM and PS-*b*-PNIPAM block copolymers. PNIPAM macro-RAFT agent, styrene and AIBN were dissolved in 1,4-dioxane by stirring at room temperature. Styrene was purified by vacuum distillation right before the polymerization. Samples were transferred to ampoules by using syringes. After three successive freeze–pump–thaw cycles, the solutions were heated to 70 °C by using a temperature controlled oil bath. Polymerization was allowed to proceed for 48 hours. Then the reaction was stopped by cooling in liquid nitrogen. 1,4-Dioxane was evaporated using a rotary evaporator. The polymer was dissolved in THF and precipitated in cold water several times to remove unreacted PNIPAM macro-RAFT agent until no homopolymer peak was found in the GPC elugram and precipitated twice from diethyl ether to remove unreacted styrene. The copolymers were dried in a vacuum oven at 35 °C (Table 1). ^{1}H NMR (400 MHz, $CDCl_3$): δ = 6.2–7.1 (5H, m, Ph), 4.0 (1H, s, –NCH–), 0.8–2.5 (3H, m, –CH–CH_2– for PS and 9H, m, –CH_3, –CH–CH_2– for PNIPAM) (Fig. S4†).

Membrane preparation

A 20 wt% polymer solution, which was prepared from a *N*-methyl-2-pyrrolidone (NMP) and tetrahydrofuran (THF) mixture with a volume ratio of 4 : 6, was poured onto a glass substrate and a thin film of polymer was formed using a manual film applicator with a gate height of 200 μm. After a certain evaporation time, the polymer film was transferred into a non-solvent bath (water). The polymer film was left in this bath for at least four hours. For atomic force microscopy (AFM) and scanning electron microscopy (SEM) analyses, a small portion of this film (1 × 1 cm) was cut and fixed on a Si wafer with double-sided tape and dried in a vacuum oven overnight at 40 °C. For permeability analysis, the membrane film was stored in demineralized water and cut into the desired dimensions just before the measurements.

Characterization

^{1}H and ^{13}C nuclear magnetic resonance (NMR) spectroscopy measurements were carried out on a Bruker AMX-400 spectrometer (400 MHz) at room temperature. The ratio between PS and PNIPAM blocks in the BCP was determined by comparing the integral of the aromatic PS protons at 6.2–7.1 ppm (5H, m, Ph) to the lone PNIPAM proton at 4.0 ppm (1H, s, –NCH–). Theoretical PS weight fractions calculated by taking yield values as conversions and experimental PS weight fractions obtained from NMR analysis were compared to evaluate the control of the polymerization in the block copolymer (Table 1). The discrepancy between the theoretical and experimental PS fractions can be attributed to material losses during purification processes.

Gel permeation chromatography (GPC) of PS macro-RAFT agents and their copolymers was run using a set-up consisting of an Agilent Technologies 1200 series gel permeation chromatograph, a PLgel 5 μm Mixed-D column (M_w range 200–400 000 Da, Polymer Laboratories Ltd) and an Agilent 1200 differential refractometer. The column was calibrated using PS standards. Each polymer sample was injected into

the tetrahydrofuran eluent at 30 °C and a flow rate of 1 mL min^{-1}. Molecular weight (number average molecular weight) ($\bar{M}_n$) and PDI values of PS macro-RAFT agents, and PDI values of PS-*b*-PNIPAM-*b*-PS block copolymers were calculated with Omnisec software V4.6. GPC of PNIPAM macro-RAFT agents and their copolymers was run on a Viscotek GPCmax equipped with 302 TDA model detectors, using a guard column (PSS-GRAM, 10 μm, 5 cm) and two analytical columns (PSS-GRAM-1000/30 Å, 10 μm, 30 cm) at a flow rate of 1 mL min^{-1} in dimethyl formamide (containing 0.01 M LiBr) at 50 °C. Poly(methyl methacrylate) standards were used for calibration of the column. $\bar{M}_n$ and PDI of PNIPAM macro-RAFT agents, and PDI of block copolymers (PNIPAM-*b*-PS-*b*-PNIPAM and PS-*b*-PNIPAM) were calculated using Omnisec software by using refractive index and light scattering signals, respectively. $\bar{M}_n$ of all block copolymers were calculated using the $\bar{M}_n$ of their macro-RAFT agents obtained from GPC and the block ratios obtained from NMR results.

For SEM measurements, the samples were placed on flat aluminum stubs with double-sided adhesive, conducting carbon tape. Samples were coated with a 10 nm layer of tungsten using a Leica EM SCD 500 sputter-coater. SEM images were recorded on an FEI Magellan 400 field-emission SEM at an acceleration voltage of 2.0 kV. For the SEM of cross-sectional films, samples were fractured in liquid nitrogen and mounted onto 90° SEM stubs with the cross-section facing upwards.

The surface morphology of the films was analyzed with a Bruker Multimode 8 AFM instrument using the Nanoscope V ScanAsyst imaging mode. DNP-10 model non-conductive silicon nitride probes with a spring constant of 0.24 N m^{-1} (Bruker) were used. Images were recorded at 1.50 Hz and processed using NanoScope Analysis 1.5 software. At least three different regions on the same film sample were probed to assure that the obtained surface morphology was representative for the entire sample. Before analysis, membrane films were cut into small pieces and fixed on Si wafers of 1 × 1 cm size using double sided tape and dried in vacuum oven at 40 °C overnight.

Permeability experiments

Permeability of the membranes was studied using a dead-end filtration set-up by measuring the flux of Milli-Q pure water at different pressures (1–3 bar). The membrane was cut into a round shape with a diameter of 2.5 cm, and subsequently placed in an Amicon type filter cell with a volume of 40 mL. The cell was connected to a pressure vessel filled with Milli-Q pure water, where pressure was applied using compressed nitrogen. The cell and the vessel were heated to specific temperatures ranging from 20 °C to 50 °C by placing them inside larger vessels filled with water which were heated using temperature controlled heating plates. To ensure a stable temperature, the cell was stored at a specific temperature for half an hour before the measurement. For all experiments, the membranes were placed on top of a non-woven fabric that acted as an additional mechanical support. Because the non-woven fabric consists of relatively large voids and has a high permeability value (~750.000 L m^{-2} h^{-1} bar^{-1}), we assumed that it had no influence on the results of the permeability experiments. The permeability (L m^{-2} h^{-1} bar^{-1}) was calculated as the ratio of the flux over the applied pressure as shown in eqn (1), where V is the permeate volume (L), A is the membrane area (m^2), t is the time (h), J is the permeate flux (L m^{-2} h^{-1}) and ΔP is the pressure change along the membrane (bar). For the temperatures higher than 20 °C, permeability results were corrected by multiplying the results with the relative change in the dynamic viscosity of water given at the specified temperature compared to that of water at 20 °C. Error bars of the flux and permeability measurements in Fig. 4 and 5 were obtained by using the standard deviations which were calculated from the average permeability values for five different pressure values.

$$\text{Permeability} = V/(A \cdot t \cdot \Delta P) = J/\Delta P \quad (1)$$

Results and discussion

In this study, we optimized the synthesis of PS-PNIPAM BCPs to obtain high molecular weights and PS majority fractions. These features are preferential for membrane fabrication using SNIPS: a high molecular weight will ensure a suitable viscosity for the SNIPS process and both features will provide mechanical stability of the membrane. To obtain the desired polymers we compared two routes: in route 1, a PS macro-RAFT agent was extended with NIPAM and in route 2, a PNIPAM macro-RAFT agent was extended with styrene using two different types of RAFT agent. Thiocarbonyl compounds as RAFT agents can be shown in a generalized structure as Z–C(=S)–S–R where R acts as the leaving group which initiates a new polymer chain and Z is the group responsible for reactivity and radical stability; this group can also be written as SR′ for the trithiocarbonate RAFT agents used in our work. The difunctional BDAT and monofunctional DTMA RAFT agents (Scheme 1) were chosen because of their suitable R and Z groups for the polymerization of styrene and NIPAM, as both give a good stability and sufficient reaction rates for each block.[43] Scheme 1 represents the synthesis routes that were used.

Synthesis and optimization of homopolymers and copolymers

According to the literature, the optimal route for RAFT polymerization of PS-PNIPAM BCPs using trithiocarbonates is to start with styrene polymerization and extension with NIPAM (reaction (1) in Scheme 1).[34,44,45] It is reported that the polymerization of styrene from a PNIPAM macro-RAFT agent causes retardation of the styrene polymerization due to slow initiation, slow fragmentation of the intermediate radicals and/or irreversible termination reactions.[44] Higher PDI values were obtained in case a PNIPAM macro-RAFT agent was used for the PS-PNIPAM copolymer synthesis as compared to the use of a PS macro-RAFT agent when a dithiocarbonate RAFT agent was used.[45] Therefore, our initial choice was to synthesize a PS macro-RAFT agent first and subsequently polymerize NIPAM from this macro-RAFT agent to obtain PS-PNIPAM copolymers as shown in reaction (1) in Scheme 1.

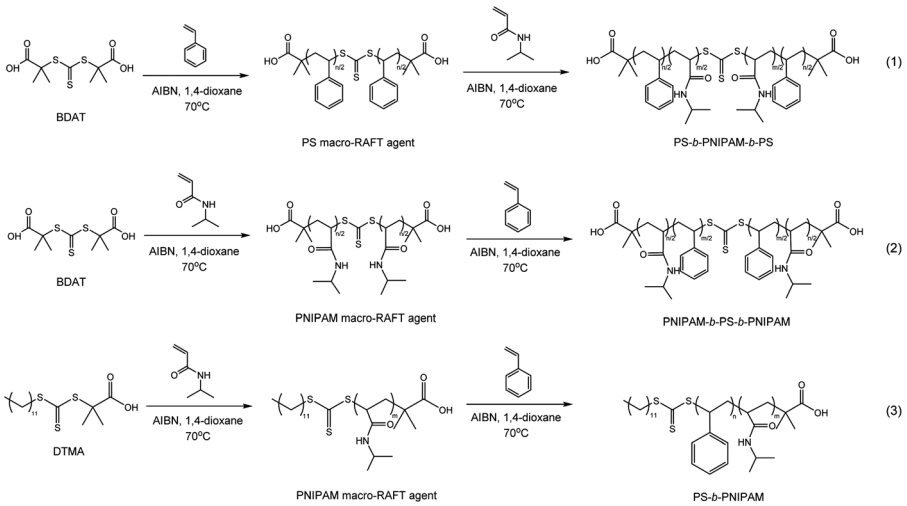

Scheme 1 Synthesis routes of the BCPs (1) PS-*b*-PNIPAM-*b*-PS, (2) PNIPAM-*b*-PS-*b*-PNIPAM, and (3) PS-*b*-PNIPAM.

Since we aim for high molecular weight PS-PNIPAM copolymers and large PS volume fractions, the initial monomer concentration ($[M]_0$), the ratio of initial monomer and chain transfer agent concentrations ($[M]_0/[CTA]_0$), consequently molecular weight of PS macro-RAFT agent were increased compared to the previously reported literature on PS-PNIPAM copolymer synthesis.[34] The molecular weight can be as well augmented by increasing the reaction time (t), and decreasing the ratio of initial chain transfer agent and initiator concentrations ($[CTA]_0/[I]_0$). Although a decreased $[CTA]_0/[I]_0$ value improves the rate of polymerization, this parameter also preserves the controlled manner of the polymerization reaction, therefore it should be kept at an optimum value. Since long reaction times and low $[CTA]_0/[I]_0$ values typically result in high PDI values, a balance for these parameters had to be found to achieve a low PDI, high molecular weights and acceptable yields. This resulted in a $[M]_0/[CTA]_0$ ratio of 1915 and a ratio of $[CTA]_0/[I]_0$ ratio of 10 and a reaction time of 24 h as the optimum values for the desired properties of the PS macro-RAFT agent. Table S1† lists all the synthesized PS macro-RAFT agents. Optimum conditions were reached for PS-9 having $\bar{M}_n$ = 92 kDa, PDI = 1.21 and yield = 16%.

An inherent disadvantage is that since we aim for BCPs with a large PS fraction, the chemical difference between the PS macro-RAFT agent and the copolymer became smaller when the PS fraction was increased. Thus, removal of PS macro-RAFT agent residue by precipitation became more difficult which resulted in a large decrease in the yield, plus theoretical and experimental PS fractions deviated strongly from each other. At the end, no copolymerization reaction took place (see CP-4 in Table 1). Therefore, here the second concomitant disadvantage is the difficulty for the monomers to reach the active center located at the middle of the chain due to hindrance and/or hydrophobicity of the already long active chain which inhibited the copolymerization reaction. It has been observed before by Wong *et al.* that longer macro-RAFT agent chains decrease the reaction rate, resulting in very low reaction yields.[46] Since synthesis route (1) did not result in optimal yields,[42,43] we switched the order and first synthesized the PNIPAM macro-RAFT agent and extended the polymer with styrene to obtain PS-PNIPAM BCPs which are shown in reactions (2) and (3) in Scheme 1.

Similar as for the PS macro-RAFT agent synthesis, for the PNIPAM macro-RAFT agent synthesis, a higher $[M]_0$ and a higher $[M]_0/[CTA]_0$ ratio led to higher molecular weights (Table S2†). Extension of the reaction times resulted in higher PDI values due to the possible side reactions, thus four hours of reaction was selected to obtain polymers with both low polydispersity, the desired molecular weights and high yields. Hence, PNIPAM macro-RAFT agents having $\bar{M}_n$ = 25–40 kDa, PDI = 1.03–1.10 were synthesized with 80% yields, which were significantly higher than the yield of PS macro-RAFT agents that was only around 10–20%.

The extension of the PNIPAM macro-RAFT agent with styrene was optimized, using a $[CTA]_0/[I]_0$ ratio of 10 (Table 1). However, due to slower kinetics of styrene polymerization, higher reaction times of 48 h were necessary, which resulted in acceptable yields with low polydispersities.

In addition, starting with the polymerization of PN-3, we changed the RAFT agent from the difunctional BDAT (reaction (2) in Scheme 1) to the monofunctional DTMA (reaction (3) in Scheme 1) (Table S2†). When DTMA was used as the RAFT agent, we obtained PS-*b*-PNIPAM diblock copolymers, following reaction route (3) in Scheme 1. We found that PDI values of the resulting PS-*b*-PNIPAM copolymers were decreased when DTMA was used (compare CN-1 (BDAT) with CN-2 (DTMA) in Table 1). Thus, the yield of the polymerization of styrene from PNIPAM macro-RAFT agent was found to be significantly higher than the yields obtained for polymerization of NIPAM with PS macro-RAFT agent with more consistent PDI values of 1.30–1.40 (Table 1). Experimentally determined PS fractions

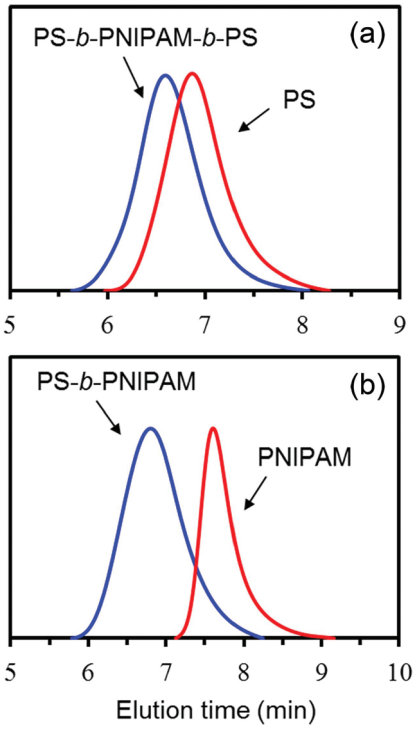

Fig. 1 GPC elugrams of (a) CP-1 and its homopolymer PS-1, (b) CN-3 and its homopolymer PN-5.

match well with the theoretical PS fractions indicating a well-controlled reaction.

Typical GPC elugrams of the PS and PNIPAM macro-RAFT agents and their copolymers are given in Fig. 1. These monomodal GPC curves indicate that there is no evidence of any residual PS and PNIPAM macro-RAFT agents in the copolymers and suggest homo- and block copolymers were synthesized with relatively narrow molecular weight distributions. The peaks were found to be almost symmetrical with a slight tailing in the case of PNIPAM macro-RAFT agents which is probably due to the interaction of the polymers with the column material in GPC. As PS does not interact with the column material, the tailing is less pronounced for the PS macro-RAFT agents. As a conclusion, we found that reaction route (3) is preferred, in case a high molecular weight PS-PNIPAM block copolymer with a high PS volume fraction is desired with high yields and low polydispersity values.

Membrane fabrication by SNIPS

A high molecular weight PS-PNIPAM block copolymer with high PS volume fraction is required to obtain mechanically stable free-standing membranes. Therefore, CN-3 with a $\bar{M}_n$ of 194 kDa, f_{PS} of 83 wt% and PDI of 1.34 was selected as the most suitable block copolymer for membrane production.

A successful SNIPS process is dependent on many parameters such as block copolymer type, block length, molecular weight, polymer concentration, type of solvent/solvent mixtures, type of non-solvent, evaporation time, temperature of polymer solution and non-solvent bath and solvent content in non-solvent bath.[22] The type of solvent is one of the most important parameters for SNIPS, due to the significant effects on the final material properties. *N*-Methyl-2-pyrrolidone (NMP) is one of the most commonly used solvents in commercial phase inversion membrane production.[47,48] Tetrahydrofuran (THF) is also frequently used for the preparation of block copolymer membranes, due to its high volatility, and its ability to create ordered morphologies.[11,17,18,20,37,49–51] For example, for the PS-*b*-P4VP system, it is well-known that THF plays an important role in the pore formation.[22] Therefore, to produce the membranes we applied a solvent combination of both water-miscible NMP and THF, with a volume ratio of 4 : 6, because this combination seemed most promising in preliminary screening experiments. Water was used as the non-solvent.

Since the solubility parameters of PS and PNIPAM are similar in value (PS: 22.49 and PNIPAM: 22.89 $MPa^{1/2}$),[52,53] they were not used directly to comment on the solvent selectivity. In order to interpret the solvent selectivity more accurately, we calculated the Flory-Huggins interaction (χ) parameters using Hansen solubility parameters of each block-solvent combination (Table 2). (Details on the calculation of χ parameters can be found in the ESI.†) Comparing the χ parameters of the block-solvent interactions, indicates that NMP is a PS selective and THF is a PNIPAM selective solvent. According to the vapor pressure values of the solvents given in Table 2, THF will evaporate faster than NMP from the cast polymer film. For an NMP : THF volume ratio of 4 : 6, increasing the evaporation time will result in evaporation of more THF which consequently results in a more viscous and more PS selective solvent system. During evaporation, a PS matrix is formed and due to poor affinity of PS with water, PS precipitates when the viscous polymer film is transferred to the non-solvent.[54]

AFM images in Fig. 2 show the morphology changes of the membrane film as a function of evaporation time. For the evaporation times of 0 and 10 seconds, the polymer solution still contained a high amount of solvent. When the film was transferred to the non-solvent bath, the remaining solvent in the cast film was exchanged with water resulting in an open porous structure with a small number of worm-like cylinders and possibly spherical micelles underneath them. As the evaporation time was extended to 15–30 seconds, the viscosity of the polymer solution increased, the cylinders got closer, fused together and formed branched worm-like structures. Plus, the

Table 2 χ parameters of the block-solvent interactions calculated from Hansen solubility parameters (see ESI) and vapor pressure of the solvents

		THF	NMP
χ parameters	PS	0.78	0.92
	PNIPAM	0.46	1.35
Vapor pressure at 25 °C (kPa)		21.6	0.04

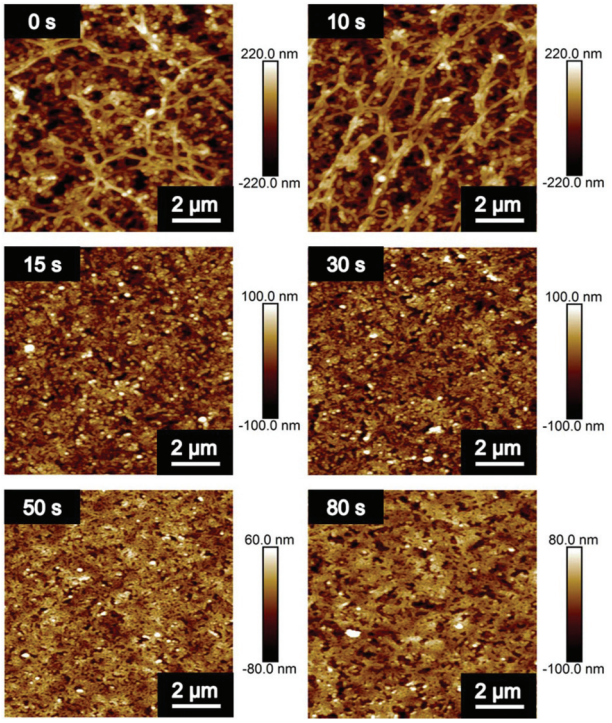

Fig. 2 AFM images showing the effect of evaporation time on the membrane morphology.

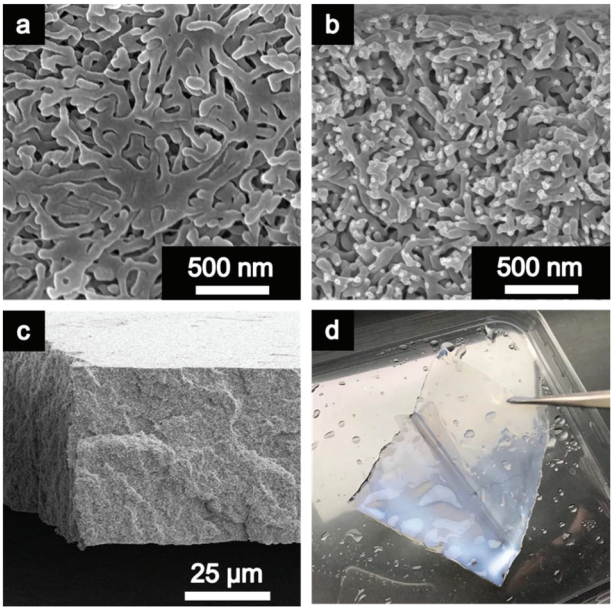

Fig. 3 SEM images of the membrane prepared using 80 s of evaporation time: (a) the surface, (b) the cross-section, (c) a 3D view and (d) a picture of the membrane.

roughness of the films started to decrease. For even longer evaporation times (50–80 seconds), the distances between the worm-like cylinders became even smaller, and a compact structure with nanopores was obtained consistent with the evaporation time-dependent SNIPS results reported by Phillip *et al.*[18] Films prepared with long evaporation times exhibited a smoother surface than the films prepared with shorter evaporation times. In addition, more opaque films were obtained for shorter evaporation times and films became more transparent when the evaporation time was increased. This difference in transparency of the films may be due to differences in pore sizes. When the size of the pores is larger than the wavelength of visible light (380–700 nm), films appear white due to light scattering and as they are lower than the wavelengths of visible light, films appear more transparent.[55]

Fig. 3a shows an SEM image of the membrane surface prepared using an evaporation time of 80 seconds. The image clearly indicates that a nanoporous surface is obtained. The SEM image of the cross-section of the membrane in Fig. 3b demonstrates that similar worm-like cylinder characteristics and interconnected nanopores are present throughout the total thickness of the film. These similar characteristics may be due to the long evaporation time of 80 seconds causing a large amount of solvent evaporation in the polymer solution. Therefore, the self-assembly of the BCPs also took place throughout the film to form cylindrical micelles with interconnected nanopores. The total film thickness was found to be 50 μm (±5 μm) (Fig. 3c) and the membrane was free-standing with a transparent/cloudy appearance (Fig. 3d).

Permeability measurements. In order to investigate the thermo-responsive properties of the membrane, we first studied membrane permeability at two different temperatures, one below (at 20 °C) and one above (at 50 °C) the LCST of PNIPAM (32 °C). The water flux through a membrane is determined by the applied pressure and the membrane permeability. However, for a true comparison of the membrane permeability, or pressure normalized flux, for different temperatures, the permeability also needs to be normalized for the temperature-dependent changes in viscosity of the water passing through the membrane at an elevated temperature. This is analogue to the established methods of membrane resistance calculations.[56] Therefore, we argue that this correction is required in order to properly analyze the changes of the membrane alone. To eliminate the effect of a decreased water viscosity at 50 °C on the flux values, viscosity corrected flux values were obtained by multiplying the flux results with the relative change in dynamic viscosity of water at 50 °C compared to that of water at 20 °C. Fig. 4a shows the change in flux values at 20 °C, flux values which are viscosity corrected at 50 °C and uncorrected at 50 °C as a function of pressure. A linear flux increase is expected for all membrane systems when the pressure increases. This linear relation between flux and pressure for both temperatures demonstrates the mechanical stability of the membrane, as compaction or rupture of the membrane would have led to strong deviations from linearity. The slope of the line for viscosity corrected flux values at 50 °C was still considerably bigger than the slope at 20 °C which clearly demonstrates the thermo-responsive character of the membrane.

We also studied the permeability increase at several temperatures between 20 °C and 50 °C at a pressure change of 1 bar as shown in Fig. 4b. Here, only viscosity corrected permeability

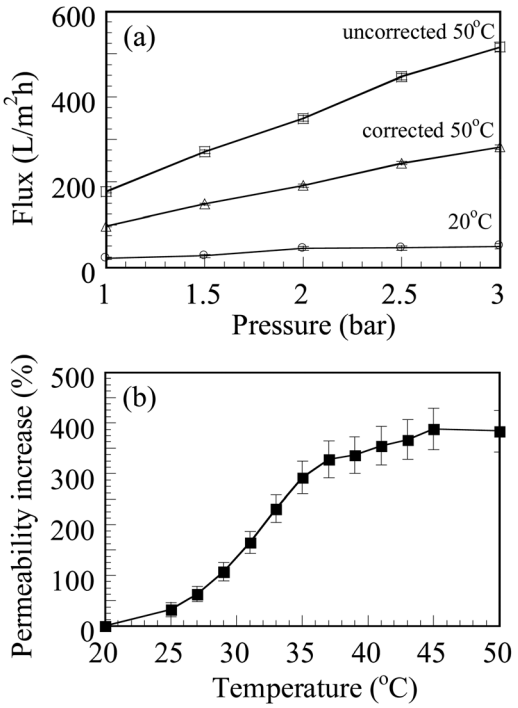

Fig. 4 (a) Flux measurements of the membrane at 20 and 50 °C as a function of pressure. Curves with circles, triangles and squares correspond to the flux values at 20 °C, viscosity corrected at 50 °C and uncorrected at 50 °C, respectively. (b) Increase in permeability as a function of temperature at 1 bar.

values are indicated. The transition mainly occurred between 26 °C and 38 °C, with the steepest permeability increase around the LCST of PNIPAM. The permeability was increased by almost 400%. These results demonstrate that the thermo-responsive behavior of the membrane is a result of the collapsing PNIPAM chains at the LCST of the polymer. This behavior also suggests that the pores of the membrane were coated with PNIPAM domains.[18]

Reversibility of the membranes was tested by measuring the permeability for several temperature cycles (*i.e.* switching between 20 and 50 °C) (Fig. 5). Here, similarly as shown in Fig. 4a, both viscosity corrected and uncorrected permeability values show that the thermo-responsive behavior is an outcome of the chain collapse of PNIPAM above its LCST. Identical permeability values were obtained for each temperature cycle demonstrating that the thermo-responsive property of the membrane is fully reversible.

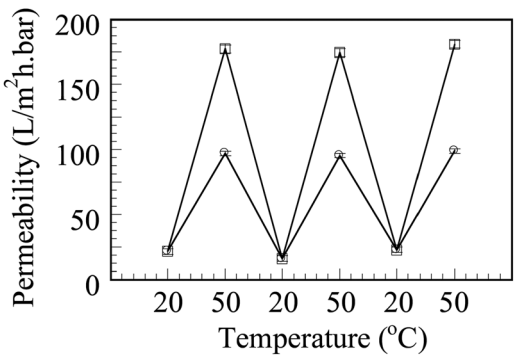

Fig. 5 Reversibility of thermo-responsive behavior of the membrane showing both viscosity corrected (circles) and uncorrected (squares) permeability values.

Conclusions

Well-defined high molecular weight PS-PNIPAM BCPs with large PS volume fractions were successfully synthesized. The optimal route to obtain this copolymer is by synthesizing a PNIPAM macro-RAFT agent first and extending the chain with styrene. SNIPS method was used for the first time to produce free-standing nanoporous membranes from PS-*b*-PNIPAM copolymers. The membranes had a worm-like cylindrical morphology with nano-sized pores, and showed thermo-responsive behavior and the thermo-responsive behavior was fully reversible. To the best of our knowledge, the production of a fully reversible thermo-responsive block copolymer SNIPS membrane has not been reported before. Membranes with fully reversible thermo-responsive character offer prospects for further development of advanced easy-to-clean membrane applications.

Acknowledgements

This research forms part of the research programme of the Dutch Polymer Institute (DPI), project #766 (Dutch Polymer Institute, P.O. Box 902, 5600 AX Eindhoven, The Netherlands). Electron microscopy work was performed at the Wageningen Electron Microscopy Centre (WEMC) of Wageningen University & Research.

References

1 M. Ulbricht, *Polymer*, 2006, **47**, 2217–2262.
2 Q. Yang, H. H. Himstedt, M. Ulbricht, X. Qian and S. Ranil Wickramasinghe, *J. Membr. Sci.*, 2013, **430**, 70–78.
3 J. I. Clodt, V. Filiz, S. Rangou, K. Buhr, C. Abetz, D. Höche, J. Hahn, A. Jung and V. Abetz, *Adv. Funct. Mater.*, 2013, **23**, 731–738.
4 K. Pan, X. Zhang, R. Ren and B. Cao, *J. Membr. Sci.*, 2010, **356**, 133–137.
5 F. Schacher, T. Rudolph, F. Wieberger, M. Ulbricht and A. H. E. Müller, *ACS Appl. Mater. Interfaces*, 2009, **1**, 1492–1503.
6 E. J. Vriezekolk, K. Nijmeijer and W. M. de Vos, *J. Membr. Sci.*, 2016, **504**, 230–239.
7 Z. Wang and Y. Wang, *Macromolecules*, 2016, **49**, 182–191.
8 C. Hörenz, C. Pietsch, A. S. Goldmann, C. Barner-Kowollik and F. H. Schacher, *Adv. Mater. Interfaces*, 2015, **2**, 1500042.
9 S. Mondal and S. R. Wickramasinghe, *Sep. Purif. Technol.*, 2012, **90**, 231–238.

10 H. H. Himstedt, K. M. Marshall and S. R. Wickramasinghe, *J. Membr. Sci.*, 2011, **366**, 373–381.
11 F. Schacher, M. Ulbricht and A. H. E. Müller, *Adv. Funct. Mater.*, 2009, **19**, 1040–1045.
12 Y.-C. Chen, R. Xie and L.-Y. Chu, *J. Membr. Sci.*, 2013, **442**, 206–215.
13 I. Tokarev and S. Minko, *Soft Matter*, 2009, **5**, 511–524.
14 D. Wandera, S. R. Wickramasinghe and S. M. Husson, *J. Membr. Sci.*, 2010, **357**, 6–35.
15 X. Chen, C. Shi, Z. Wang, Y. He, S. Bi, X. Feng and L. Chen, *Polym. Compos.*, 2013, **34**, 457–467.
16 S. P. Nunes, A. R. Behzad, B. Hooghan, R. Sougrat, M. Karunakaran, N. Pradeep, U. Vainio and K.-V. Peinemann, *ACS Nano*, 2011, **5**, 3516–3522.
17 Y. Gu and U. Wiesner, *Macromolecules*, 2015, **48**, 6153–6159.
18 W. A. Phillip, R. Mika Dorin, J. r. Werner, E. M. V. Hoek, U. Wiesner and M. Elimelech, *Nano Lett.*, 2011, **11**, 2892–2900.
19 S. P. Nunes, R. Sougrat, B. Hooghan, D. H. Anjum, A. R. Behzad, L. Zhao, N. Pradeep, I. Pinnau, U. Vainio and K.-V. Peinemann, *Macromolecules*, 2010, **43**, 8079–8085.
20 B. P. Tripathi, N. C. Dubey, S. Choudhury, F. Simon and M. Stamm, *J. Mater. Chem. B*, 2013, **1**, 3397–3409.
21 S. Yu, Z. Chen, J. Liu, G. Yao, M. Liu and C. Gao, *J. Membr. Sci.*, 2012, **392–393**, 181–191.
22 K.-V. Peinemann, V. Abetz and P. F. W. Simon, *Nat. Mater.*, 2007, **6**, 5.
23 S. P. Nunes, *Macromolecules*, 2016, **49**, 2905–2916.
24 W. A. Phillip, M. A. Hillmyer and E. L. Cussler, *Macromolecules*, 2010, **43**, 7763–7770.
25 L. Li, L. Schulte, L. D. Clausen, K. M. Hansen, G. E. Jonsson and S. Ndoni, *ACS Nano*, 2011, **5**, 7754–7766.
26 R. M. Dorin, H. Sai and U. Wiesner, *Chem. Mater.*, 2014, **26**, 339–347.
27 H. Ahn, S. Park, S.-W. Kim, P. J. Yoo, D. Y. Ryu and T. P. Russell, *ACS Nano*, 2014, **8**, 11745–11752.
28 M. A. Hillmyer, in *Block Copolymers II*, ed. V. Abetz, Springer, Berlin, Heidelberg, 2005, pp. 137–181, DOI: 10.1007/12_002.
29 E. A. Jackson and M. A. Hillmyer, *ACS Nano*, 2010, **4**, 3548–3553.
30 Y. Zhang, J. L. Sargent, B. W. Boudouris and W. A. Phillip, *J. Appl. Polym. Sci.*, 2015, **132**, 41683.
31 A. S. Zalusky, R. Olayo-Valles, J. H. Wolf and M. A. Hillmyer, *J. Am. Chem. Soc.*, 2002, **124**, 12761–12773.
32 C. Park, J. Yoon and E. L. Thomas, *Polymer*, 2003, **44**, 6725–6760.
33 J. K. Kim, S. Y. Yang, Y. Lee and Y. Kim, *Prog. Polym. Sci.*, 2010, **35**, 1325–1349.
34 A. Nykänen, M. Nuopponen, A. Laukkanen, S.-P. Hirvonen, M. Rytelä, O. Turunen, H. Tenhu, R. Mezzenga, O. Ikkala and J. Ruokolainen, *Macromolecules*, 2007, **40**, 5827–5834.
35 Y. Tang, K. Ito, L. Hong, T. Ishizone and H. Yokoyama, *Macromolecules*, 2016, **49**, 7886–7896.
36 K. Scott, *Handbook of Industrial Membranes*, Elsevier, Oxford, UK, 1995.
37 X. Qiu, H. Yu, M. Karunakaran, N. Pradeep, S. P. Nunes and K.-V. Peinemann, *ACS Nano*, 2013, **7**, 768–776.
38 Z. Yi, P.-B. Zhang, C.-J. Liu and L.-P. Zhu, *Macromolecules*, 2016, **49**, 3343–3351.
39 M. Gallei, S. Rangou, V. Filiz, K. Buhr, S. Bolmer, C. Abetz and V. Abetz, *Macromol. Chem. Phys.*, 2013, **214**, 1037–1046.
40 J. Chiefari, Y. K. Chong, F. Ercole, J. Krstina, J. Jeffery, T. P. T. Le, R. T. A. Mayadunne, G. F. Meijs, C. L. Moad, G. Moad, E. Rizzardo and S. H. Thang, *Macromolecules*, 1998, **31**, 5559–5562.
41 J. T. Rademacher, M. Baum, M. E. Pallack, W. J. Brittain and W. J. Simonsick, *Macromolecules*, 2000, **33**, 284–288.
42 C. H. A. Dieter Schlüter and J. Sakamato, *Synthesis of Polymers: New Structures and Methods*, Wiley-VCH, Weinheim, 2012.
43 J. T. Lai, D. Filla and R. Shea, *Macromolecules*, 2002, **35**, 6754–6756.
44 A. M. Bivigou-Koumba, J. Kristen, A. Laschewsky, P. Müller-Buschbaum and C. M. Papadakis, *Macromol. Chem. Phys.*, 2009, **210**, 565–578.
45 A. V.-R. a. A. Licea-Claveríe, *J. Mex. Chem. Soc.*, 2011, **55**, 21–32.
46 K. H. Wong, T. P. Davis, C. Barner-Kowollik and M. H. Stenzel, *Polymer*, 2007, **48**, 4950–4965.
47 K. Kneifel and K. V. Peinemann, *J. Membr. Sci.*, 1992, **65**, 295–307.
48 M. Sadrzadeh and S. Bhattacharjee, *J. Membr. Sci.*, 2013, **441**, 31–44.
49 S. Rangou, K. Buhr, V. Filiz, J. I. Clodt, B. Lademann, J. Hahn, A. Jung and V. Abetz, *J. Membr. Sci.*, 2014, **451**, 266–275.
50 E. J. Vriezekolk, K. Nijmeijer and W. M. de Vos, *J. Membr. Sci.*, 2016, **504**, 230–239.
51 M. Cetintas and M. Kamperman, *Polymer*, 2016, **107**, 387–397.
52 H. Ahmad, *J. Macromol. Sci., Part A*, 1982, **17**, 585–600.
53 C. M. Hansen, *Hansen Solubility Parameters: A User's Handbook*, CRC Press, U.S.A, 2000.
54 V. Abetz, *Macromol. Rapid Commun.*, 2015, **36**, 10–22.
55 W. Schärtl, *Light Scattering from Polymer Solutions and Nanoparticle Dispersions*, Springer-Verlag, Berlin. Heidelberg, 2007.
56 M. Mulder, *Basic Principles of Membrane Technology*, Kluwer Academic Publishers, Dordrecht, The Netherlands, 2004.